International Journal of Disaster Risk Reduction 103 (2024) 104314

Contents lists available at ScienceDirect

International Journal of Disaster Risk Reduction

journal homepage: www.elsevier.com/locate/ijdrr

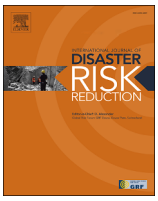

Seismic risk assessment for the downtown of the city of Blida, Algeria

Fouzi Bellalem [a], Sergio Molina [b, d, *], James Daniell [c], Said Maouche [a], Abdelhak Talbi [a], Mourad Mobarki [a], Hayet Ymmel [a], Hamou Djellit [a]

[a] Centre de Recherche en Astronomie, Astrophysique et Géophysique, CRAAG, BP 63, 16340, Bouzaréah, Algeria
[b] Multidisciplinary Institute for Environmental Studies Ramon Magalef (IMEM), University of Alicante, Alicante, Spain
[c] Geophysikalisches Institut, Karlsruhe Institute of Technology (KIT), Hertzstraße 16, Karlsruhe, 76187, Germany
[d] Dept. Applied Physics, Faculty of Sciences, University of Alicante, Alicante, Spain

ARTICLE INFO

Keywords:
Blida city
Seismic risk assessment
Earthquake scenarios
SELENA
Sensitivity analysis

ABSTRACT

Blida (Algeria) is characterized by a high level of seismic exposure and vulnerability due to its dense population and the presence of aging buildings. The historical earthquake that occurred in 1825, with a moment magnitude (Mw7.1), underscored the urgent need for a thorough assessment of seismic risk in the area. Here, an extensive study conducted in downtown of the city of Blida to evaluate seismic risk and its consequences is presented. Geounits 141 and 148 emerged as the most severely affected in all the simulated earthquake scenarios indicating severe damage and casualties mainly for closest earthquakes (Blida and Bounaian, both with moment magnitude Mw7.1) but also for furthest earthquakes as Mouzaia El Affroun (Mw6.6), and Hammam Melouane (Mw6.5). The sensitivity analysis demonstrated the importance of the selection of the performance point computation method (improved displacement coefficient method -IDCM, modified capacity spectrum-MADRS, and nonlinear analysis method-N2) and the choice of the ground motion prediction equation. IDCM results are less influenced by the choice of the GMPE, but they provide higher damage results expressed as a mean damage ratio. Moreover, the study estimated potential human impacts in the Blida region, highlighting varying levels of impact on different geounits under different earthquake scenarios. The study's primary findings from seismic risk assessments in the studied region highlight its high susceptibility to earthquakes and can be summarized as follows: The mean damage ratio will be 52.6% ± 1.4%, 50.9% ± 1.6%; 31.8% ± 3.4% and 21.4% ± 3.1% for the Blida, Bounaian, Mouzaia El Affroun and Hammam Melouane earthquakes respectively.

1. Introduction

Algeria, like many other countries, has experienced significant natural disasters, including earthquakes, leading to societal disruptions and substantial economic losses. These disasters have a particularly significant impact on urban areas with concentrated social infrastructures and underground lifeline facilities. The region of Blida in Algeria is characterized by relatively high seismic activity, with numerous destructive earthquakes recorded over the past two centuries. The strongest earthquake in the Blida region occurred on March 2, 1825, (Mw7.1), resulting in extensive damage and a death toll of approximately 7000 people [1–10]. Another significant earthquake struck the region on January 2, 1867, (Mw6.6), causing substantial loss of life and property [8–11].

* Corresponding author. Multidisciplinary Institute for Environmental Studies Ramon Magalef (IMEM), University of Alicante, Alicante, Spain.
E-mail address: sergio.molina@ua.es (S. Molina).

https://doi.org/10.1016/j.ijdrr.2024.104314
Received 6 September 2023; Received in revised form 2 February 2024; Accepted 5 February 2024
Available online 13 February 2024

The downtown area of Blida (Fig. 1) is marked by a significant population and a large number of old buildings, including the historical centre named Ouled Soltane, commonly known as "Douirette". This area represents the oldest district, predominantly comprised single or two-storey buildings dating back to the colonial era. These coexist with a mix of recent and Ottoman-era buildings in an advanced state of decay [12]. Consequently, it faces a substantial seismic exposure and inherent vulnerability.

To effectively assess and mitigate the seismic risks in downtown Blida, a comprehensive assessment must consider various factors. These include seismic risk elements such as the geological and tectonic characteristics of the region, the proximity to active faults, soil conditions and site amplification effects, structural vulnerability of buildings, and the population density and demographics. By considering these factors, it becomes possible to develop a thorough understanding of the potential impact of earthquakes in the city and implement appropriate measures to enhance the resilience and safety of downtown Blida.

In recent years, numerous studies conducted in Algeria have focused on predicting potential seismic damage to urban structures ([13–19], among others). These studies have utilized physics-based methods, including empirical fragility analysis, to assess how buildings respond during earthquakes. These approaches involve obtaining data from imposed scenarios in various regions, such as northern Algeria, and using fragility curves or matrices to estimate the vulnerability and potential damage levels of different building types, with a specific focus on residential buildings. Despite the common use of physics-based methods by the aforementioned authors, these studies have employed varied tools and techniques for earthquake risk assessment. Often, they neglected the integration of geotechnical data for evaluating local site conditions, such as the shear wave velocity of the uppermost 30-m layer (Vs30). Therefore, it is crucial to emphasize that incorporating geotechnical data, specifically Vs30, is an effective approach for predicting local site amplification. Besides, similar studies have already been performed for urban areas outside of Algeria ([20–24], amongst others).

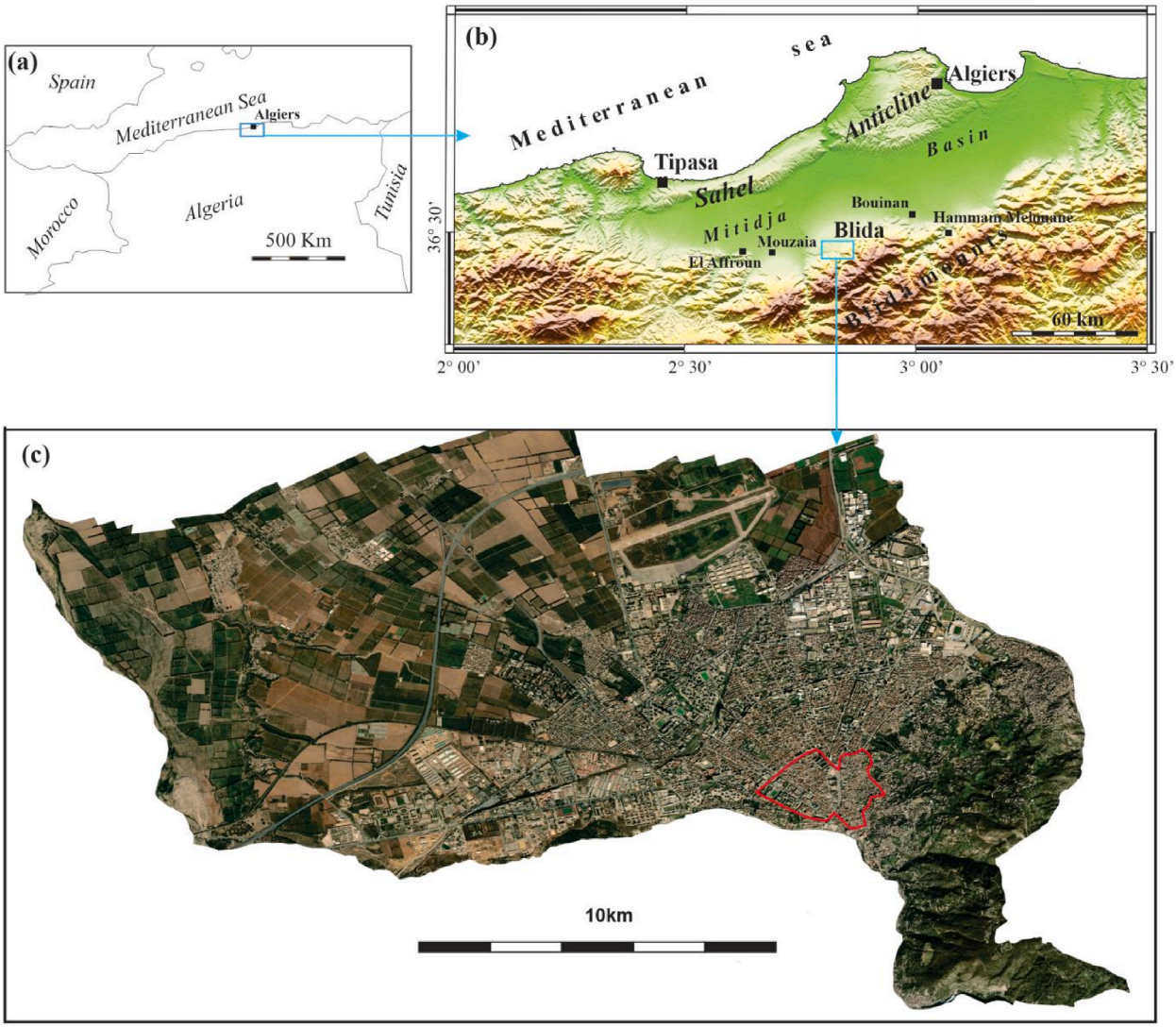

Fig. 1. Geographical situation (a) inset indicating the global localisation (b) geomorphic setting of the Blida zone surrounding area and (c) boundaries of downtown Blida city (red delimitation). (For interpretation of the references to colour in this figure legend, the reader is referred to the Web version of this article.)

In this study, we aim to address the existing knowledge gap by conducting a comprehensive assessment of seismic risk in downtown Blida, Algeria. The main objective is to provide valuable insights into earthquake vulnerability and consequences in the area, contributing to a more comprehensive understanding of the seismic risks faced by downtown Blida. To achieve an accurate seismic evaluation at the urban level, establishing an appropriate taxonomy is crucial to allow the classification of different buildings in Blida into a set of model building types with their corresponding capacity and fragility. In our study focused on downtown Blida, Algeria, we have adopted the typological classes or taxonomy proposed by Lagomarsino and Giovinazzi [25]. This classification assigns specific classes to buildings in the region of interest, taking into account the height of the buildings, the seismicity of the region, and the ductility classes. The chosen classification is based on the main characteristics of buildings in the Euro-Mediterranean region, making it relevant to our study.

We used fragility and capacity curves developed within the EU-FP5 RISK-UE project for the chosen taxonomies [25]. These curves provide valuable information about the probability of damage for each of the four damage levels (Slight, Moderate, Extensive and Complete) for a given building type. To compute the damage, we used SELENA, a software tool specifically designed for this purpose [26]. Furthermore, we compared the impact of four earthquake scenarios: Mouzaia-El Affroun Fault F1 (Mw6.6), Blida Fault F2 (Mw7.1), Bouinan Fault F3 (Mw7.1), and Hammam Melouane Fault F4 (Mw6.5) into our analysis. Integrating these scenarios with our procedures aimed to comprehensively assess the potential impact of earthquakes on Blida city and its inhabitants. This approach enabled us to evaluate the damage and losses depending of the magnitude and the distance to the city, thereby gaining a deeper understanding of the potential consequences. Ultimately, our findings provide valuable insights into the seismic resilience of downtown Blida, since it can contribute to the development of effective strategies for mitigating earthquake risks.

2. Seismotectonic setting

Numerous studies related to the seismicity, seismological and seismotectonic in the southern border of the Mitidja basin have been carried out to better understand the tectonic activity and assess its seismogenic potential [27–31]. The active deformation model of the Mitidja Basin remains a matter of debate. However, the recent re-evaluation of the historical seismicity and seismological analyses of recent earthquakes occurring on its southern edge has provided a better insight into the characteristics of its active tectonics [9,27,31,32]. The Blida reverse fault system represented by a more than 100 km segmented fault and its offshore continuation, may likely be the origin of the strong Zemmouri 2003, Mw6.9 earthquake. This tectonic scarp exhibits an impressive topographic offset, sometimes exceeding 1000 m along the northern base of the Blida Tell Atlas [29]. Fig. 2 illustrates the four different fault segments capable of generating destructive earthquakes that could cause damage in the city of Blida. Historically, one of the most devastating earthquakes in the Blida area was that of the 1867 Mouzaia-El Affroun earthquake. This event could be linked to the E-W Mouzaia-El Affroun reverse fault segment which displays left-lateral strike-slip movement on its SW end [27]. The assessed magnitude of this earthquake shows great uncertainty but could be 5.5 ≤Ms ≤ 6.5 [9]. Towards the east the Blida, Bouinan and Hammam Melouane segments are also sources of the ongoing seismicity, particularly the earthquakes of 1854, 1908 and 1961 with Mw5.5 [9,11,33,34]. Additionally, a more recent earthquake occurred in 2013 with a magnitude of Mw5.0 [35]. The maximum magnitudes in Blida and its

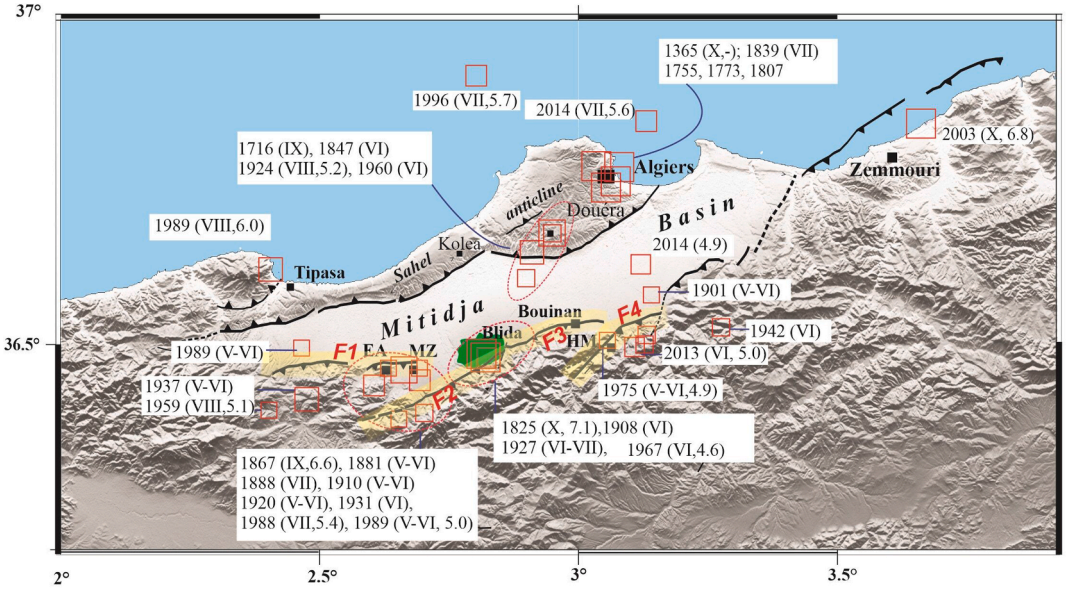

Fig. 2. Seismotectonic map illustration of major structural features in the Blida zone (Green) and neighbouring area. The plotted seismicity represents the most significant earthquakes that have occurred in the Mitidja basin from 1365 to the present day. Each seismic event is represented by a transparent box, indicating the year of its occurrence, the epicentral intensity I_0, and its magnitude (M) if available; (de): destructive event. The faults MEA, Blida, Bouinan and HM (F1 to F4) are highlighted in transparent yellow boxes (modified from Refs. [9,27]). (For interpretation of the references to colour in this figure legend, the reader is referred to the Web version of this article.)

vicinity have been evaluated using three different approaches: historical records, deterministic methods (employing Wells and Coopersmith relationships [36]), and expert opinions. Additionally, depth information derived from field observations and measurements are summarized in Table 1. The most significant earthquakes from 1760 to present day are plotted in Fig. 2, with epicentral intensities (I_0), and magnitudes, where available. Due to its shallow nature and proximity to the highly urbanized city of Blida, such seismicity could cause significant damage.

3. Methodology

3.1. Soil characterization

As illustrated in Fig. 3, the study area was divided into 16 cadastral sections according to the standards established by the National Soil Conservation and Cadastre Office. These divisions facilitate administrative pocesses, enabling a comprehensive inventory of the current building stock and the incorporation of demographic data from a preliminary housing survey conducted by the office for National Statistics (ONS). To characterize the local site conditions of each cadastral section, the shear wave velocity (Vs30) of the uppermost 30-m layer was selected as the key parameter. This approach effectively predicts local site amplification, as indicated by various references [37–41]. The seismic-refraction method was chosen to investigate the distribution of seismic velocity and changes in layer thickness within the study area. By calculating wave propagation velocities in different soil layers, seismic refraction provides a precise depiction of subsoil's structural arrangement [42–44]. This technique is applicable to shallow survey depths (from a few meters to hundreds of meters) and is particularly useful in engineering and hydrogeology problems [45–47]. This paper employed the seismic refraction technique along three profiles (Fig. 3), using 24 geophones to acquire seismic wave data with a dominant frequency of 10 Hz. The seismic waves were recorded using a 24-channel PASI-16SG seismograph as the data logger, enabling the data to be stacked. A standard 63.5 kg weight drop at a fixed height served as the seismic source to generate the compressional wave velocity. The intercept time method was processed using WinSism™ (Geosoft) version-13 software. Due to site constraints, the total number of geophones varied based on the available space. For seismic survey lines PS-01 and PS-02, the space between geophones was set at 4 m to achieve a profile length of 92 m (24 geophones x 4 m), while for seismic survey line PS-03, the space between geophones was 3 m, resulting in a profile length of 69 m (24 geophones x 3 m). The average shear wave velocity up to a depth of 30 m, commonly referred

Table 1
Four scenarios of fault segments in the Blida zone considered in the analysis and respective source parameters. The depth is deduced using the average depth of the significant earthquakes of the Tell Atlas.

ID	Faults	Depth (Km)	Mw	Fault mechanism	Dip (°)	Fault orientation (°)	Approach used for Mw estimation
F1	Mouzaia -El Affroun (MA)	10	6.6	Reverse	60	85	Historical
F2	Blida (BL)	10	7.1	Reverse	50	70	Historical
F3	Bouinan (BN)	10	7.1	Reverse	50	80	Expert Opinion
F4	Hammam Melouane (HM)	10	6.5	Reverse	55	70	Deterministic

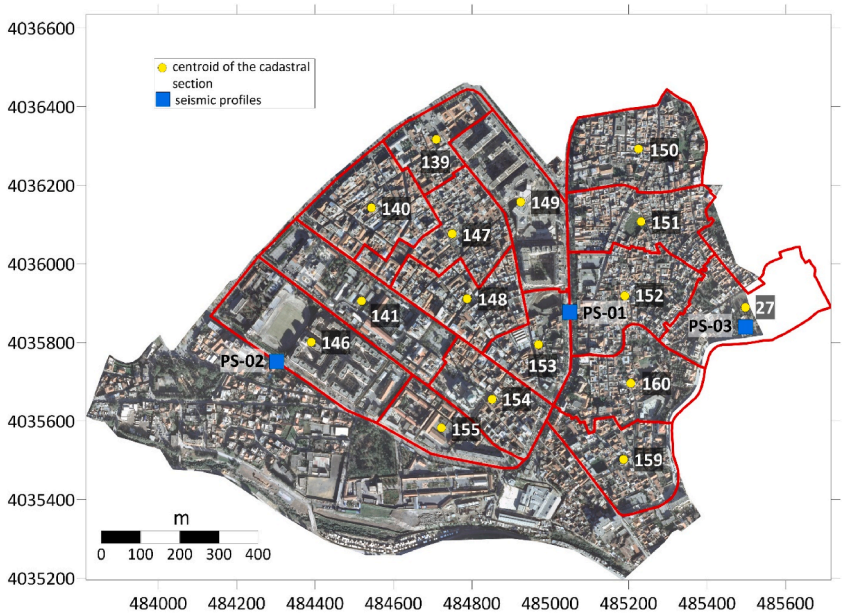

Fig. 3. Representation of the urban area of Blida downtown as discretized by 16 cadastral sections on orthorectified aerial photographs with a pixel resolution of 12-m. The blue squares represent the seismic profiles and the yellow dots indicate the centroid of each cadastral section. (For interpretation of the references to colour in this figure legend, the reader is referred to the Web version of this article.)

to as Vs30, was then calculated. The findings, as displayed in Table 2 indicate that the distribution of Vs30 decreases gradually in an easterly direction, ranging from 555 m/s at PS-03 to 539 m/s at PS-02. According to the Algerian Building Code (RPA, 2003 [48]), these values fall under the category of stiff soil and are characterized by average Vs30 values ranging from 400 m/s to 800 m/s, corresponding to the S2 soil type classification in the Algerian building code. These findings, along with soil section maps (see Fig. 4), were used to interpolate Vs30 measurements to other parts of the study area. Consequently, for all units in the study area, an average value of Vs30 was assigned to the centroid of each cadastral section.

3.2. Ground motion models

To perform seismic hazard assessment, damage and loss evaluation, and the design of seismic-resistant buildings at a specific location, a site-specific response spectrum is necessary. This spectrum can be derived from ground motion models, also known as ground motion prediction equations (GMPEs). GMPEs describe the median and the variability of ground-motion amplitudes, depending on factors such as the magnitude, site-source distance, site conditions, and other parameters. In this study, three new generations of GMPEs were employed to calculate Peak Ground Acceleration (PGA) and spectral acceleration values, within each cadastral section through deterministic analysis. To select the GMPEs for this study, a list of approximately 800 published seismic ground motions (estimating PGA and elastic response spectral ordinates, published between 1964 and early 2021) was compiled by Ref. [49]. From this list, only the most reliable GMPEs were retained, based on strong motion data obtained from Algeria ([50] [LA18]) and other regions worldwide with comparable seismotectonic conditions ([51] [AK13] and [52] [BR14]). It is worth mentioning that LA18, AK13 and BR14 are all based on moment magnitude Mw, which is the preferred magnitude scale. Additionally, all three of these GMPEs provide site effect coefficients, as well as a reduced prediction standard deviation (σ). The weights allocated to each GMPE, as shown in Table 3, were determined through expert judgment, following the general recommendations outlined in Ref. [53].

3.3. Earthquake scenarios for Blida and logic tree development

To properly evaluate the impact of future earthquakes in downtown Blida city and its inhabitants, a comprehensive understanding of the seismicity due to the active faults is crucial, along which choosing corresponding earthquake scenarios (in terms of magnitude, depth and fault location). Considering the seismotectonic context explained in section 2, four different earthquake scenarios on different faults (Table 1) were chosen: Mouzaia-El Affroun Fault F1 (Mw6.6), Blida fault F2 (Mw7.1), Bouinan Fault F3 (Mw7.1) and Ham-

Table 2
Data acquisition details along the profiles and results of Vs30 measurements for the three seismic survey lines.

Designation		Coordinates WGS84/UTM Zone 31S		Length of the profile (m)	Interval space (m)	Performed measurements	Vs30 (m/s)
		East (X) (m	North (Y) (m)				
PS-01	start	484968	4036195	92	4	Vp + Vs	545
	end	484906	4036127				
PS-02	start	484222	4036071	92	4	Vp + Vs	555
	end	484321	4036003				
PS-03	start	485420	4036152	69	3	Vp + Vs	539
	end	485425	4036214				

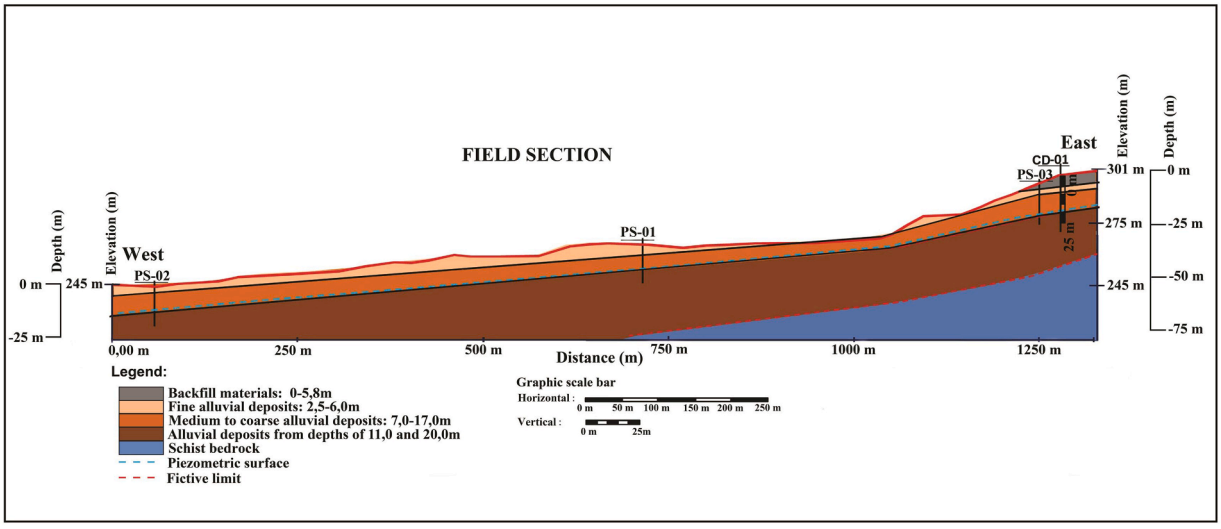

Fig. 4. Sketch of cross section of the soil profile along E-W. CD-01 The core (wash/rotary) drilling is used to determine the sub-surface profile, by obtaining the SPT–N value of soil.

Table 3
Ground motion prediction models (GMPEs) used in the study.

GMPE	Distance	Area	Weight in the logic tree
[50] [LA08]	Hypocentral	Algeria + Europe + W. USA	0.4
[51] [AK13]	Joyner-Boore	Europe & Middle East	0.3
[52] [BR14]	Joyner-Boore	Worldwide shallow-crustal	0.3

mam Melouane Fault F4 (Mw6.5). By running simulations on these different scenarios, we can discuss the damage and loss scenarios in the city but how these results may vary for each earthquake rupture. The results can also assist in identifying the most damaged areas within the city, aiding the development and implementation of effective emergency plans and mitigation strategies. It is important to note that the seismic damage and loss results are always affected by epistemic uncertainties, which can be considered and analyzed using a logic tree. We considered the uncertainty in the earthquake source simulation four different earthquakes and for each one we included the uncertainty in the ground motion prediction equation used (Table 3) and the performance point computation method (see section 3.7). The GMPEs were assigned different weights, with LA18 having a weight of 40% while AK13 and BR14 had a weight of 30% each. This indicates that LA18's predictions are considered more critical or reliable than those of AK13 and BR14. The performance point method was equally weighted. Only one soil model, corresponding to stiff soil, was used. Fig. 5 presents a diagram of the logic tree computation scheme used in this study, so each simulated earthquake will provide nine different results (one for each branch of the logic tree with corresponding weights).

3.4. Building and population data collection

The concept of earthquake vulnerability is crucial in predicting the average damage that buildings are likely to experience on a large scale in the event of a given magnitude. Earthquake vulnerability analysis also identifies of the buildings and structures at a regional, city, or county level that may suffer higher damage from a given ground motion. This analysis is essential for determining which buildings may need reinforcement or retrofitting, making it a crucial first step in seismic risk mitigation efforts. Vulnerability analysis includes factors at risk (physical, social and economic) and the nature of associated risk such as damage to structures and systems and human losses [54]. To conduct a seismic vulnerability assessment, building inventory and population information must be included. However, other elements (social, economic, etc.) would have only a minor impact on the assessment results if they were not included. For the case study in Blida, a comprehensive building inventory survey was conducted using a rapid visual screening method across a small area (~94 ha). This survey covered all buildings within the zone and involved in-depth investigations into various attributes, including building structural type, occupancy class, total floor area, number of stories, seismic vulnerability characteristics, construction period, and typology. This in-situ fieldwork allowed the gathering of essential data without the need for structural calculations. Upon completion, this information was integrated with GIS-based city planning database for advanced risk analysis, along with other geographical layers such as demographic data from a preliminary housing survey conducted by the Office for National Statistics (ONS) in 2020 and the location of traffic lanes. In total, 2607 buildings were surveyed across 16 geographical units, constituting the building stock. The residential general occupancy is the most significant, both in terms of exposure and building count, due to the large number of collective housing and single-family dwellings, which constitute 83.6% of all buildings. Table 4 shows the number of buildings, dwellings, and the population in each cadastral section, obtained from GIS building inventory data for the downtown Blida.

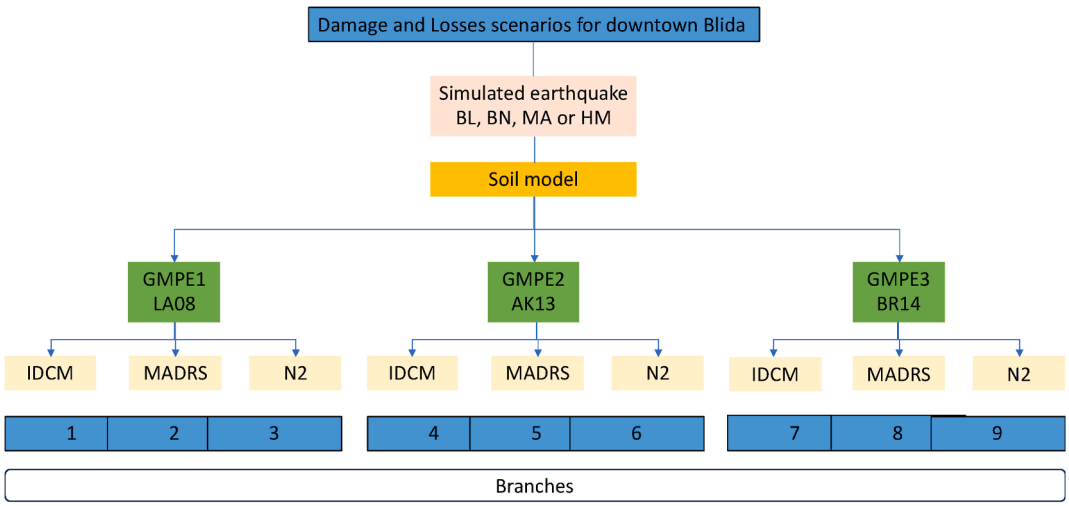

Fig. 5. Schematic of the logic tree computation scheme used in the study.

Table 4
Detailed information regarding number of buildings, number of dwellings, and the population for each cadastral section.

GEOUNIT	CENTROID OF GEOUNIT		NUMBER OF BUILDINGS	NUMBER OF DWELLINGS	POPULATION	BUILT AREA (m^2)
	X(m)	Y(m)				
27	485414	4036207	150	164	805	67300
139	484626	4036635	90	145	679	35410
140	484461	4036461	196	424	1962	60500
141	484435	4036224	43	106	487	74300
146	484307	4036120	47	346	1592	90300
147	484666	4036395	219	415	1917	53600
148	484704	4036230	219	467	2167	49920
149	484841	4036476	63	394	1817	66900
150	485141	4036611	236	274	1331	70400
151	485148	4036426	291	332	1619	59200
152	485107	4036237	347	358	1764	69500
153	484886	4036113	90	78	373	39360
154	484768	4035974	164	226	1073	48030
155	484639	4035901	52	96	445	37530
159	485104	4035821	181	188	920	53800
160	485122	4036014	219	257	1236	62900
Total			2607	4270	20187	938950

3.5. Buildings typology

To conduct an accurate seismic evaluation at the urban level, beginning with an appropriate taxonomy is crucial. Taxonomies are important as they provide a simplified way to describe the structural behaviour of existing buildings, avoiding complex structural modelling. However, it should be noted that while the grouping of model building types into taxonomies is appropriate for developing damage and losses scenarios needed for emergency management, specific infrastructures like hospitals and schools should be treated individually by structural modelling. Once a taxonomy is established, each building can be assigned to a specific typological class, a critical process for meaningful seismic evaluations at the urban scale. The expected damage during a seismic event is directly related to the building type, making this attribution process crucial. The evolution of taxonomies started from the 78 different types of structural systems proposed by ATC-13 [55] which were later named FEMA model building types [56]. These US-specific buildings influenced the global building classification system (PAGER-STR, [57]). In Europe and the Mediterranean region, the RISK-UE project also defined taxonomies for residential and historical buildings [25]. Additionally, the Global Earthquake Model has developed a worldwide taxonomy [58], defined by 13 attributes that describe specific characteristics of individual buildings. However, the GEM taxonomy requires very detailed knowledge of the buildings so in this study, we have adopted the typological classes proposed by RISK.UE [25]. This approach offers a simplified way to assign a specific class to each building in the region of interest. We selected this classification as it is based on the main characteristics of buildings in the Euro-Mediterranean region, making it relevant to our study. Table 5 presents the building typology classification adopted in this study. The classification considers three different classes of building height: Low-Rise (_L), Mid-Rise (_M), and High-Rise (_H), defined based on the number of masonry floors (_L = 1/2, _M = 3/5, _H ≥ 6) or reinforced concrete floors (_L = 1/3, _M = 4/7, _H ≥ 8). It also takes into account the seismicity of the region, with zones I (_I), II (_II), and III (_III, as well as the ductility class (-WDC = without ductility class, -LDC = low ductility class, -MDC = medium ductility class, -HDC = high ductility class) **[25]**.

Based on the building typology and height, using the nomenclature provided in Table 5, a total of nineteen model building types have been identified in downtown Blida. The number of buildings of each model type in the studied region is shown in Fig. 6.

The distribution of buildings in downtown Blida, as revealed in Fig. 6, shows that the majority of the buildings fall under the low-rise M3 and M2 types. These buildings typically have unreinforced masonry walls made of bricks and simple stone in various combinations. Notably, all these buildings were constructed before 1980 and were not designed according to any building code. Fig. 7 rep-

Table 5
Building typology classification.

Typologies	Building types	
Unreinforced Masonry	M1	Rubble stone
	M2	Adobe (earth bricks)
	M3	Simple stone
	M4	Massive stone
	M5	U Masonry (old bricks)
	M6	U Masonry – r.c. floors
Reinforced/confined masonry	M7	Reinforced/confined masonry
Reinforced Concrete	RC1	Concrete Moment Frame
	RC2	Concrete Shear Walls
	RC3	RC3 Dual System

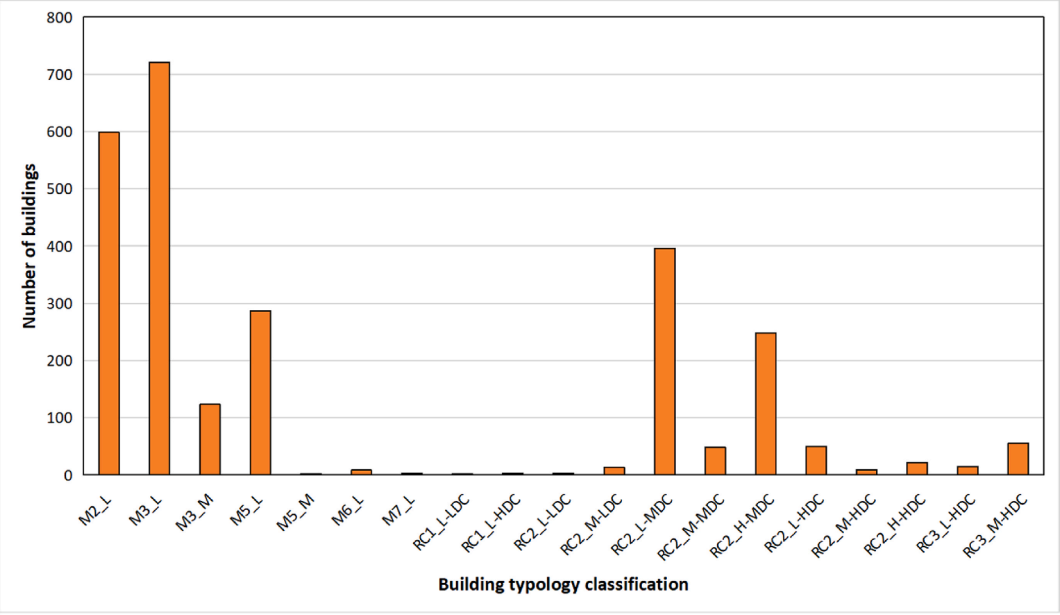

Fig. 6. Number of buildings belonging to each taxonomy that exist in downtown Blida.

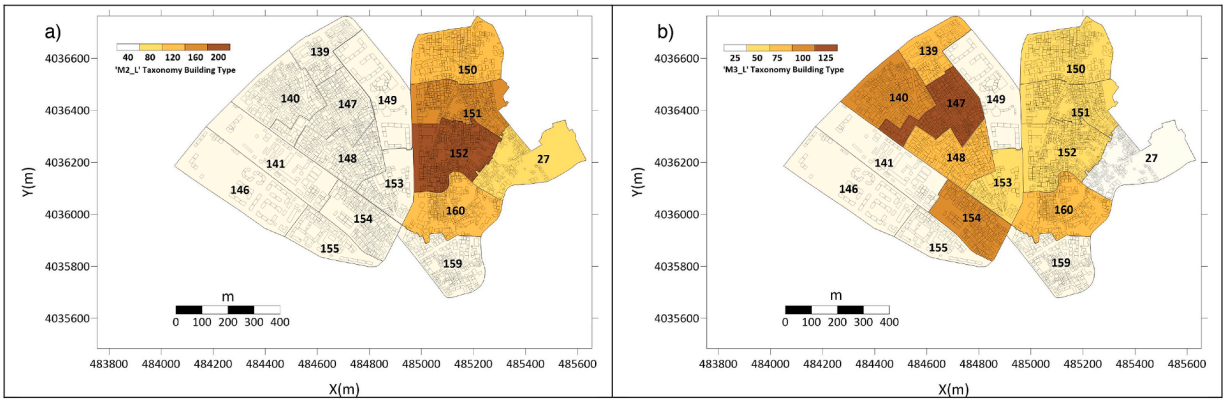

Fig. 7. The spatial distribution of un-reinforced masonry buildings is characterized by a) M2_L Taxonomy building type, and b) M3_L Taxonomy building type.

resents the distribution of the M3_L and M2_L model building types. The cadastral section 147 and 152 have the highest concentration of these model building types, respectively.

3.6. Population inventory

The concept of “population exposed to seismic hazards" refers to individuals residing in seismically dangerous areas or locations susceptible to potential property destruction of property and loss of human life resulting from seismic events [59,60]. Therefore, a population inventory is a crucial tool for assessing the impact of an earthquake on society. By creating a population inventory, it is possible to identify areas of high exposure and test the impact of different earthquake scenarios, aiding disaster preparedness.

This study utilized current population data obtained from a preliminary housing survey conducted by the Office for National Statistics (ONS) in 2020. The customary census activities of the ONS typically involve conducting surveys and interviews with individuals, households, and communities to collect demographic information, including age, sex, marital status, education level, occupation, and household composition. The results of this census allowed us to determine the number of inhabitants in each district and for the different existing typologies in the region. The number of inhabitants was deduced by leveraging the information gathered in a dedicated inventory sheet, which integrated building structural data with inhabitants per building obtained from the ONS census. This comprehensive integration facilitated the analysis, enabling the determination of the number of inhabitants for different existing typologies in the region.

Fig. 8 illustrates the ratio of the population count across different typological classes present in the studied region, namely masonry buildings (a) and reinforced concrete buildings (b) for each geounit.

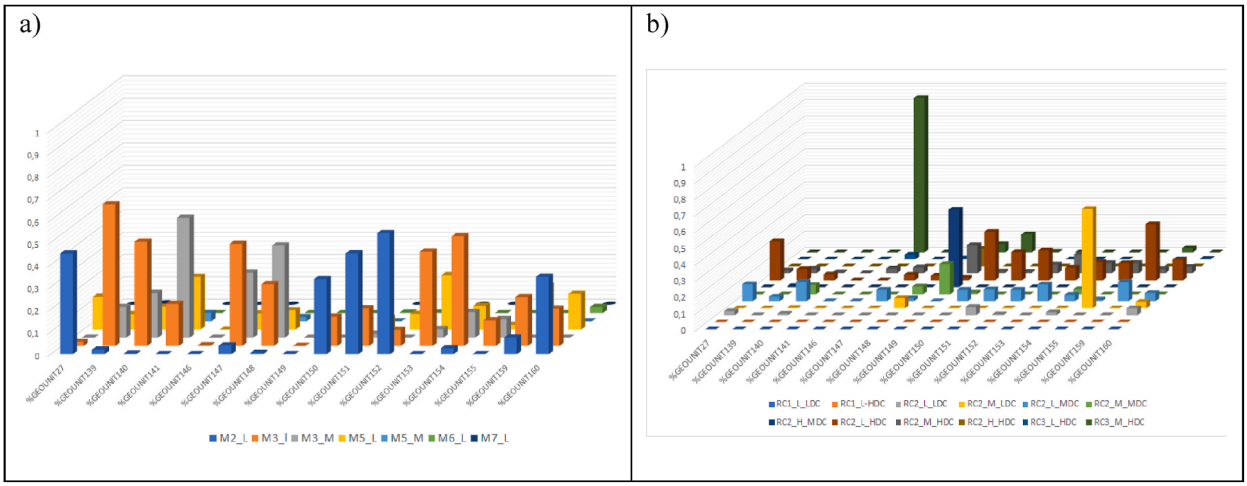

Fig. 8. Population ratio for a) masonry and b) reinforced concrete buildings in the studied region.

As observed, in most of the geounits the inhabitants are living in masonry buildings. Only geounits 146, 149 and 155 show a higher population in reinforced concrete buildings.

3.7. Fragility and capacity curves

To calculate the physical damage using different analytical methods, we employed fragility and capacity curves developed within the EU-FP5 RISK-UE project for the European building taxonomy [25]. In this study, the capacity curves were obtained from a mechanical model known as the DBV (Displacement Based Vulnerability) method, which is applicable to both masonry and reinforced concrete frame structures. The DBV method represents a building's response using a capacity curve, also known as a force-displacement curve. This curve characterizes the structural response of a building in terms of stiffness, overall strength, and ultimate displacement [61]. Our methodology incorporates three user-selectable methods for computing the performance point of each model building type due to a given specific response spectrum from the simulated earthquake and the corresponding capacity curve: the Modified Acceleration-Displacement Response Spectrum Method (MADRS) [62], the Improved Displacement Coefficient Method (IDCM) [62], and the nonlinear static method (N2) developed by Ref. [63]. These methods are included in the software SELENA [26].

Once the performance point is computed, the damage probability is obtained through fragility curves which express the probability of a building class sustaining a specific damage state (ds) when subjected to a certain level of ground motion intensity. Typically, these curves are represented by a lognormal cumulative distribution function, with a median value and logarithmic standard deviation or dispersion. The mathematical form of the fragility curves is as follows [64]:

$$P\left(d_s/S_d\right) = \Phi\left[\frac{1}{\beta_{ds}} \log\left(\frac{S_d}{S_{d,ds}}\right)\right]$$

where S_d is the spectral displacement corresponding to the performance point and $S_{d,ds}$ is the median value of spectral displacement at which the building reaches the threshold of damage state *ds* (slight, moderate, extensive and complete).

β_{ds}: standard deviation of the natural logarithm of spectral displacement for damage state *ds*,

Φ(): standard normal cumulative distribution function.

A detailed description of the different damage states (ds) previously mentioned can be found in Ref. [25].

Table 6 defines the median value of the damage state threshold spectral displacements and the log-normal standard deviations for each taxonomy and for damage state, i.e., Slight, Moderate, Extensive and Complete.

Fig. 9 shows the capacity curves for all masonry and reinforced concrete buildings used in the study. Additionally, we have also represented the fragility curve for two different typologies, illustrating how different damage states are reached earlier in masonry buildings than in reinforced-concrete building.

3.8. Mean damage ratio (MDR)

Quantifying earthquake-induced building damage is complex due to the variance in disaggregation of damage estimates for different scenarios or building typologies. To address this challenge, the Mean Damage Ratio (MDR) serves as a useful parameter for comparing risk estimation across different geounits within a city or between different cities or countries. MDR is defined as the cost ratio corresponding to each damage state, expressed as a ratio to the cost of new construction [14,65,66]. MDR is particularly beneficial for comparing risk estimation across different test beds, cities, or countries, as it remains stable and not influenced by factors such as inflation, exchange rates, and other variables that affect reconstruction and repair costs [26]. However, while MDRs have their advantages, disaggregated damage estimates are crucial for predicting social losses, such as casualties, since complete damage states (particularly collapse) result in the majority of casualties and fatalities [26,66,67].

Table 6
Spectral displacement-based fragility curve parameters for each damage state for a specific building type.

Taxonomy	$S_{d,slight}$ (cm)	β_{slight}	$S_{d,moderate}$ (cm)	β_{slight}	$S_{d,extensive}$ (cm)	β_{slight}	$S_{d,complete}$ (cm)	β_{slight}
M2_L	0.18	0.55	0.39	0.55	0.65	0.55	1.04	0.55
M3_l	0.17	0.66	0.36	0.66	0.74	0.66	1.24	0.66
M3_M	0.17	0.66	0.36	0.66	0.74	0.66	1.24	0.66
M5_L	0.20	0.64	0.42	0.64	0.84	0.64	1.40	0.64
M5_M	0.44	0.48	0.95	0.48	1.37	0.48	2.11	0.48
M6_L	0.25	0.62	0.54	0.62	1.04	0.62	1.71	0.62
M7_L	0.21	0.82	0.45	0.82	1.32	0.82	2.33	0.82
RC1_L_LDC	1.67	0.44	3.59	0.44	4.78	0.44	7.16	0.44
RC1_L_HDC	1.84	0.62	3.95	0.62	7.47	0.62	12.30	0.62
RC2_L_LDC	2.24	0.44	4.80	0.44	6.40	0.44	9.60	0.44
RC2_M_LDC	3.49	0.44	7.47	0.44	9.96	0.44	14.94	0.44
RC2_L_MDC	2.88	0.46	6.17	0.46	6.81	0.46	13.12	0.46
RC2_M_MDC	4.09	0.52	8.76	0.52	10.59	0.52	21.19	0.52
RC2_H_MDC	5.49	0.52	11.76	0.52	14.21	0.52	28.42	0.52
RC2_L_HDC	2.70	0.57	5.79	0.57	9.88	0.57	15.90	0.57
RC2_M_HDC	3.27	0.64	7.01	0.64	13.96	0.64	23.25	0.64
RC2_H_HDC	4.39	0.64	9.41	0.64	18.73	0.64	31.19	0.64
RC3_L_HDC	2.34	0.57	5.01	0.57	8.54	0.57	13.73	0.57
RC3_M_HDC	2.83	0.64	6.06	0.64	12.06	0.64	20.08	0.64

According to Ref. [26], MDR, for each geounit *i*, is computed using the following formula:

$$MDR_i = \frac{\sum_{j=1}^{mbt} DR_S^j \bullet N_{Si}^j + DR_M^j \bullet N_{Mi}^j + DR_E^j \bullet N_{Ei}^j + DR_C^j \bullet N_{Ci}^j}{N_{Ti}}$$

with:

DR_k^j : is the damage ratio of model building type j corresponding to damage state k where k = S for slight, M for moderate, E for extensive and C for complete damage,

N_{ki}^j: is the damaged built area corresponding to damage state k (S, M, E, C) the model building type j in geounit i,

N_{Ti}: is the total built area in the cadastral section or geounit i over all model building types.

A total MDR for the whole city can also be obtained using:

$$MDR = \frac{\sum_{i=1}^{geounit} \sum_{j=1}^{mbt} DR_S^j \bullet N_{Si}^j + DR_M^j \bullet N_{Mi}^j + DR_E^j \bullet N_{Ei}^j + DR_C^j \bullet N_{Ci}^j}{N_T}$$

with N_T the total built area over all model building types j and over all geounits i.

3.9. Human casualty computation method

The number of casualties due to direct structural damage for any given structural type, level of building damage, and injury severity can be calculated [26]:

$$K_i = \{Injuries\,(severity\ i)\} = \sum_{j=1}^{mbt} \sum_{k=1}^{DS} C_{i,k}^{CSR} \cdot P_{j,k} \cdot N_j^{POP}$$

$C_{i,k}^{CSR}$ casualty rate of severity i for damage state k

$P_{j,k}$: structural damage probability of the model building type j for damage state k

N_j^{POP}: number of people in model building type j

Severity of injuries goes from i = 1 light injuries (slight) to i = 2 hospitalized injuries (moderate), i = 3 life threatening injuries (heavy) and i = 4 injuries causing death (death) according to HAZUS [68].

To account for varying occupancy patterns dependent on the time of day, the SELENA methodology incorporates the calculation of casualty numbers for three distinct timeframes: nighttime, when most of the people are in the residential buildings; daytime and commuting time scenarios. For our study, we focused on the nighttime scenario, anticipating the highest number of casualties among the population located at home during this period. We assumed that during the night, 90% of Blida's population resides indoors, and 10% are outdoors.

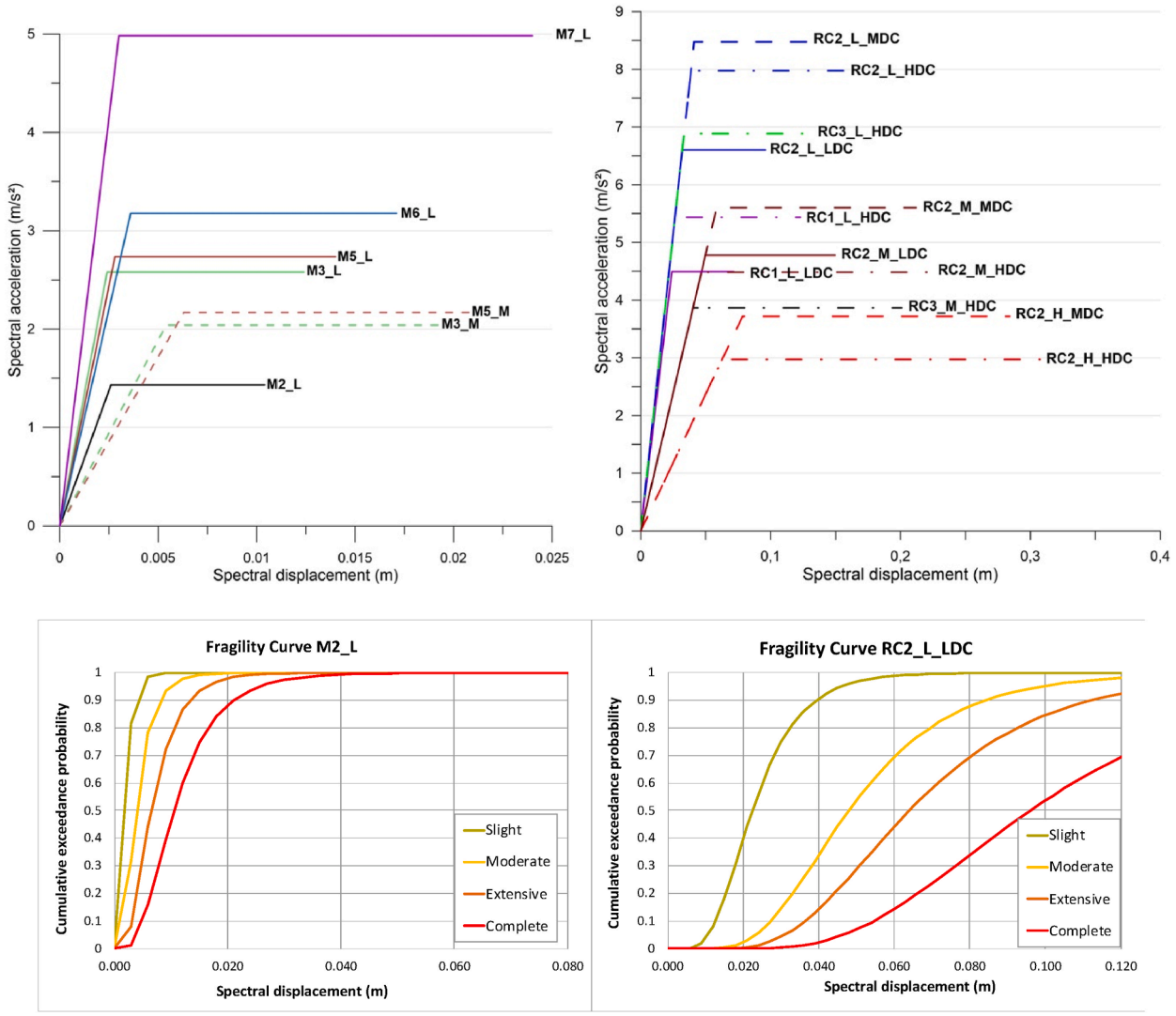

Fig. 9. Top: Capacity curves for all the masonry typologies (M) and for all the reinforced concrete typologies (RC); Bottom: Comparison of two fragility curves: masonry (M2_L) and reinforced concrete (RC2L_LDC).

4. Results and discussions

4.1. Mean damage ratio (MDR)

The analysis of the MDR offers valuable insights into the potential impact of earthquakes on buildings. Fig. 10 depicts the distribution of the mean damage ratio for each cadastral section across the four different earthquake scenarios after averaging the results obtained from the logic tree.

The findings highlight the existing significant vulnerability in the city combined with the ground motion scenarios, resulting in considerable damage due to the simulated earthquakes in the studied area. Table 7 summarizes the obtained results. The MDR results vary with the size of the earthquake and its distance from the city. The closest earthquakes, Blida (BL) and Bouanian (BN) both with Mw7.1, yield the highest MDR, ranging approximatively from 13% to 90% approximately, as the rupture area reaches the city. The Mouzia El Afroun (MA) earthquake with Mw6.6 and mean Joyner-Boore distance of 23 km impacts with MDR ranging from 2% to 63%, while the Hammam Melouane (HM) earthquake with Mw6.5 and a mean Joyner-Boore distance of 21 km results in MDRs ranging from 1% to 42%.

For all the earthquake scenarios, cadastral sections 141 and 148 exhibit the highest MDR: approximatively 90% and 75% approximately for the BL and BN earthquakes, 63% and 49% for the MA earthquake and 42% and 33% for the HM earthquake. This is attributed to the high vulnerability of these cadastral sections, as most of the buildings in these areas are masonry structures (approximately 81%), with only a 19% being reinforced concrete buildings. Conversely, cadastral districts 146 and 149 have the lowest MDR for all the earthquakes, as most of the buildings there are reinforced concrete structures (90% and 100%, respectively). Here the MDR for the closest earthquakes ranges from 12% to 18% and between 1% and 5% for the furthest earthquakes.

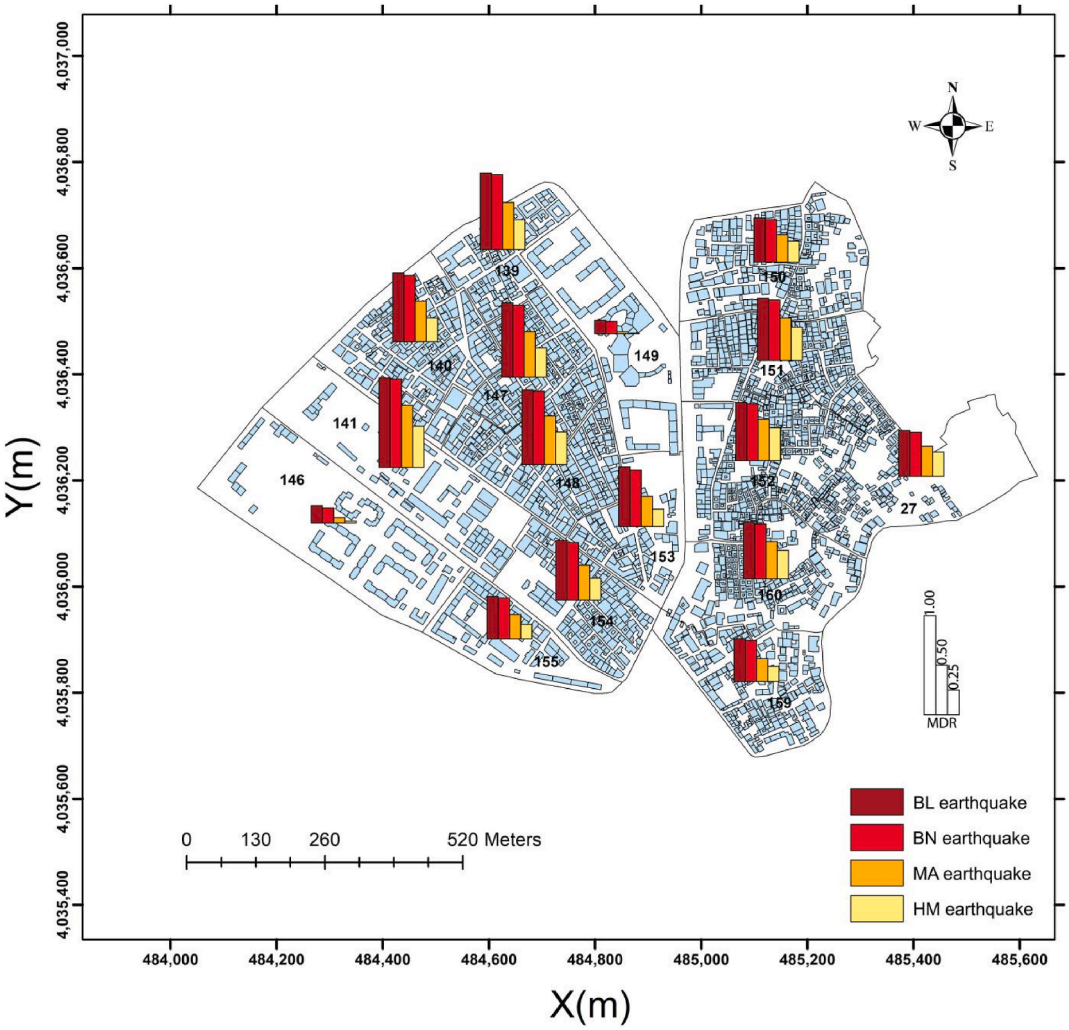

Fig. 10. Distribution of the averaged mean damage ratio per geounit for four different seismic scenarios, established using SELENA.

Table 7
Comparative analysis of averaged Mean Damage Ratios and standard deviation for geounits under different earthquake scenarios.

GEOUNIT	Mean Damage Ratio (%)			
	BL earthquake (Mw7.1)	BN earthquake (Mw7.1)	MA earthquake (Mw6.6)	HM earthquake (Mw6.5)
27	46.16 ± 0.91	44.34 ± 0.90	30.18 ± 3.36	24.39 ± 3.82
139	76.66 ± 2.90	75.05 ± 3.07	47.09 ± 3.58	29.63 ± 2.65
140	68.97 ± 2.36	66.50 ± 2.88	40.69 ± 3.54	23.69 ± 2.91
141	90.30 ± 3.33	88.96 ± 3.61	62.49 ± 10.56	41.61 ± 10.85
146	17.49 ± 0.44	15.07 ± 0.38	5.35 ± 1.52	1.84 ± 0.06
147	74.39 ± 2.51	72.34 ± 2.89	45.8 ± 4.83	29.29 ± 4.20
148	75.01 ± 2.65	73.56 ± 2.85	48.84 ± 6.99	32.72 ± 6.80
149	13.63 ± 0.32	12.52 ± 0.65	2.22 ± 0.31	0.866 ± 0.001
150	44.44 ± 0.75	42.99 ± 0.98	27.85 ± 2.58	21.30 ± 2.75
151	62.25 ± 1.1	60.73 ± 1.45	42.63 ± 4.45	33.36 ± 4.94
152	58.50 ± 0.86	56.91 ± 1.07	41.49 ± 4.63	33.14 ± 5.45
153	59.84 ± 1.77	56.71 ± 2.61	30.27 ± 1.09	17.32 ± 1.60
154	60.21 ± 1.85	57.85 ± 2.31	35.26 ± 3.41	22.21 ± 2.91
155	42.57 ± 1.55	41.04 ± 1.71	24.38 ± 2.17	14.61 ± 1.73
159	43.32 ± 1.14	41.25 ± 1.57	23.23 ± 1.83	15.28 ± 1.48
160	56.56 ± 1.11	55.04 ± 1.39	37.47 ± 4.18	28.62 ± 4.54

Therefore, these results indicate that a higher vulnerability due to the presence of existing unreinforced buildings in the city will amplify the impact of upcoming earthquakes.

4.2. Sensitivity analysis

Investigating the sensitivity of three performance point assessment procedures (IDCM, MADRS, N2) across various earthquake scenarios revealed crucial insights into the uncertainties linked with earthquake damage evaluation. Fig. 11 illustrates the sensitivity of these methods across different earthquake scenarios.

In most cases, the IDCM method computes the highest values, while the N2 method computes the lowest. The differences between the methods are usually more significant in cadastral sections with a higher MDR. Additionally, we observe that the differences between the methods increase with the distance from the earthquake. For example, the cadastral geounit 141 has a standard deviation of the MDR of 3.33% and 3.61% for BL and BN earthquakes, which increase to 10.56% and 10.85% for MA and HM, respectively.

The influence of the selection of ground motion prediction equation (GMPE) on the MDR results is also notable. Fig. 12 compares the median and percentiles obtained from the logic tree for each performance point computation method and for each earthquake. A higher or lower dispersion indicates a greater or lesser influence on the GMPE choice.

For the BL earthquake, the influence of the ground motion prediction equation is more pronounced when using the N2 method, as indicated by the larger dispersion of the results. The AK13 GMPE provides the lowest MDR, while LA18 and BR14 yield higher and closest results for all the methods. This difference in results is more pronounced with the N2 method, as the median value shifts towards the highest MDR values. Regarding the BN earthquake, with a similar Joyner-Boore distance as the BN earthquake, the results for AK13 and BR14 are the same. However, due to a slightly higher hypocentral distance, the results from LA18 are now the lowest, and those from BR14 are the highest. Again, the N2 method appears more influenced by the GMPE choice, as shown by the larger dispersion.

For the furthest earthquakes, the influence of the GMPE choice increases for all methods, with MADRS showing higher sensitivity. This trend is similar for the HM earthquake, although the dispersion between results is lower than for the MA earthquake. In this case, LA18 provides the lowest MDR values, while BR14 provides the highest.

Thus, the choice of the GMPE and the performance point computation method are both crucial when applying spectral displacement methods in the seismic risk assessment. The IDCM method appears to be less influenced by the choice of GMPE for the simulated earthquakes, although this does not necessarily indicate it provides the most accurate MDR values. The reliability and robustness of

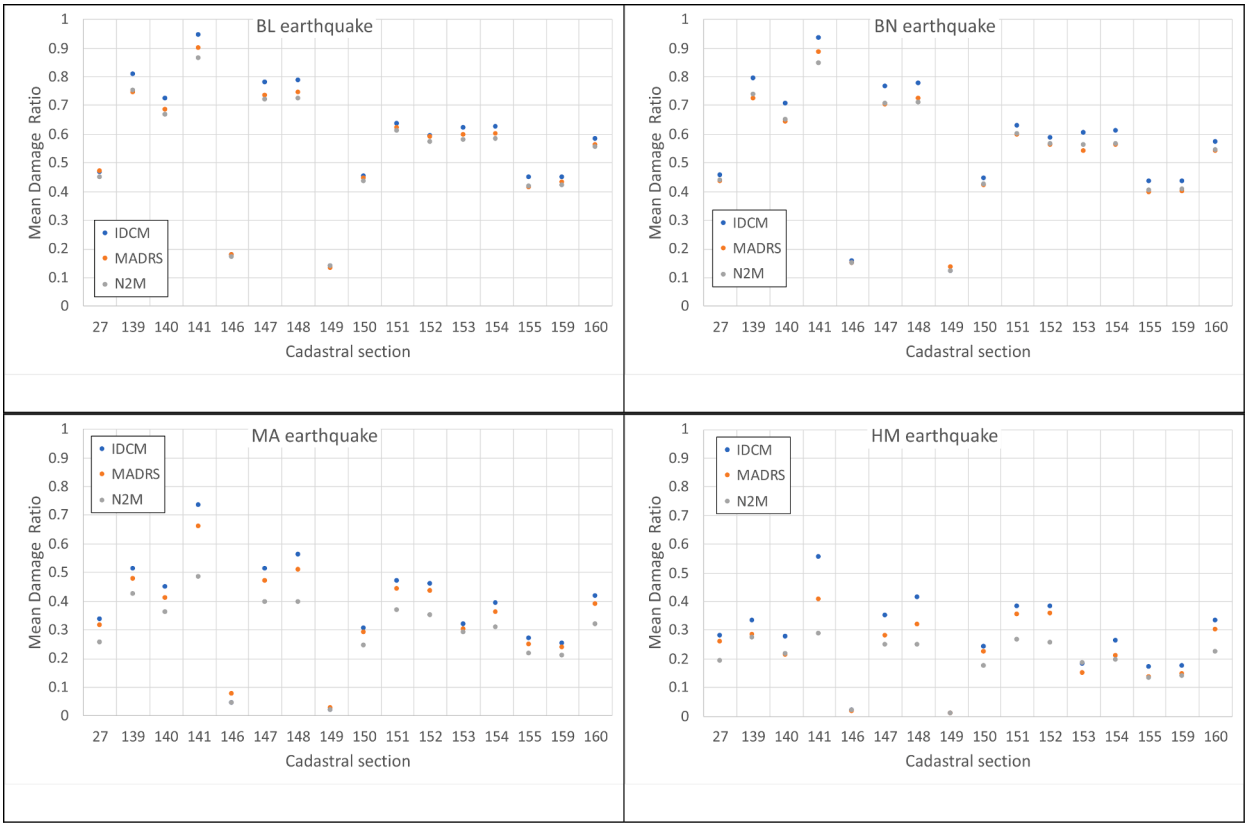

Fig. 11. Mean damage ratio obtained for each earthquake and performance point computation method.

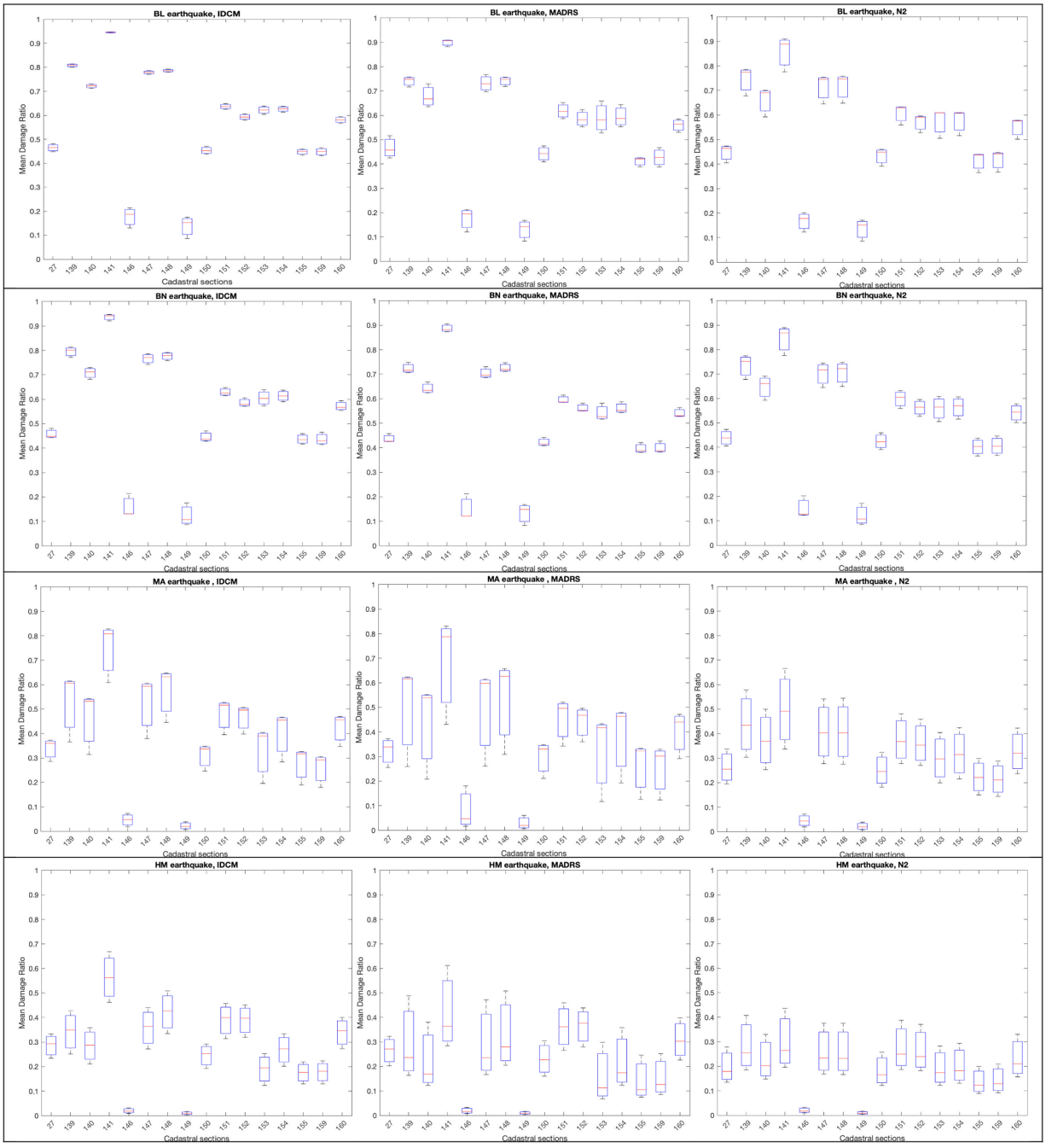

Fig. 12. Sensitivity analysis of IDCM, MADRS, and N2 methods for assessing the Mean Damage Ratio and its uncertainties due to the choice of GMPE. (BL- Blida Mw7.1 earthquake; BN- Bouinan Mw7.1 earthquake; MA- Mouzia El Afroun Mw6.6 earthquake and HM- Hammam Melouane Mw6.5 earthquake).

simplified methods for estimating displacement demand can only be assessed by comparing their results with those from a more accurate analysis (e.g. response history analysis). However, this is beyond the scope of this paper.

Finally, using the logic tree, it is possible to obtain a global mean damage ratio for the entire city. The results are summarized in Table 8.

As we observe the distance to the city and the magnitude of the earthquake significantly influence the Mean Damage Ratio (MDR). Furthermore, the uncertainty of the results increases as the distance to the city increases.

Table 8
Impact of the simulated earthquakes in the city of Blida as a function of the global Mean Damage Ratio.

Earthquake	IDCM	MADRS	N2M	Averaged
BL	54.6 % ± 1.3 %	52.3 % ± 2.6 %	51.2 % ± 3.6 %	52.6 % ± 1.4 %
BN	53.2 % ± 1.9 %	49.8 % ± 1.8 %	49.7 % ± 3.1 %	50.9 % ± 1.6 %
MA	35.2 % ± 6.2 %	32.9 % ± 9.7 %	27.2 % ± 6.9 %	31.8 % ± 3.4 %
HM	25.3 % ± 4.4 %	21.1 % ± 7.2 %	17.7 % ± 5.6%	21.4 % ± 3.1 %

4.3. Building damage assessment

In this study, we have investigated the damage percentages categorized by building taxonomy under different earthquake scenarios. Across the analyzed earthquake scenarios (Mouzaia El Affroun M_W6.6, Bouainan Mw7.1, Blida Mw7.1, Hammam Melouane Mw6.5), the masonry or unreinforced taxonomies (M2_L, M3_L, M3_M, M5_L, M5_M, M6_L and M7_L) consistently exhibit a significant percentage of complete damage (Fig. 13). This highlights how the impact of a given earthquake will be more severe in buildings with higher vulnerability.

Similarly with the MDR, the closest earthquakes (BL and BN) exhibits the highest percentage of buildings with complete damage, with values exceeding 75% for taxonomies M2_L, M3_L, M3_M, M5_L, M5_M, M6_L. Reinforced concrete buildings do not exceed the 5% of complete damage, except for the taxonomy RC1-L_DCL, which reaches 17% of complete damage. The MA earthquake causes complete damage in 76% and 66% of M2L and M3_M buildings, 9% to30% in masonry and unreinforced buildings, but no damage in reinforced concrete buildings.

The HM earthquake results in 59% and 45% of complete damage in the M2L and M3M buildings, respectively and 4% to16% in masonry and unreinforced buildings. Again, none of the reinforced concrete buildings suffer complete damage or extensive damage, except for RC1_L_LDC, which reaches 1% extensive damage.

These results underscore the importance of developing strategies to improve the seismic performance of buildings, especially the more vulnerable M2_L and M3_M taxonomies, to enhance the overall resilience of communities in earthquake-prone areas.

4.4. Human casualty assessment

This section delves into the distribution of casualties and injuries across various geounits within different earthquake scenarios, providing crucial insights into the potential consequences of seismic events on affected populations. Fig. 14 visualizes the spatial distribution of the affected population (at least severity 1 injuries) across different geounits and the histogram of total injuries in the city for each severity level (1 to 4, that is slight to death) due to each simulated earthquake. The results are also averaged using the three performance point computation methods and the three GMPEs.

The analysis of different earthquake scenarios provides valuable insights into the distribution of casualties and injuries across various geounits.

Cadastral section 148, with the highest number of inhabitants: 2167 (11% of the total populations approximately), and a significance percentage of masonry buildings, is expected to experience the highest number of affected individuals in all earthquake scenarios. The affected population (at least slight injuries) due to the BL and BN earthquakes are projected to be 351 ± 24 and 344 ± 26 inhabitants (16% of the population in the cadastral section), respectively from which with 20 ± 2 are fatalities for each scenario (around 1% of the population in the cadastral section). The MA and HM earthquakes will affect to 205 ± 58 and 123 ± 50 inhabitants, respectively (9% and 6% of the population in the cadastral section) while the fatalities will be 11 ± 3 and 7 ± 3, respectively.

As we see, the impact is similar for BL and BN due to the rupture area reaching the city, and it decreases for the HM and MA earthquakes.

Cadastral section 141 has only 487 inhabitants (2.4% of the total population) but a high mean damage ratio. Thus, its impact on the population is lower due to the reduced exposure. BL and BN earthquakes will affect 98 ± 7 and 96 ± 8 inhabitants (20% of the population in the cadastral section) and the fatalities will be 6 ± 1 and 5 ± 1 inhabitants while MA and HM affect 58 ± 16 and 33 ± 15 inhabitants (12% and 7% of the total population in the cadastral section) respectively.

We can see that although a lower exposure will imply less affected population in absolute numbers however since section 141 has a higher mean damage ratio than section 148, it will cause a higher value of affected population in terms of percentage of the total population in the section.

Local authorities should prioritize districts with higher numbers of vulnerable buildings and inhabitants for first responder rescue efforts to minimize fatalities.

While our simulations should not be seen as precise predictions, given the high uncertainty in seismic losses, they are invaluable for emergency management. Identifying the most affected cadastral sections allows emergency teams to prepare evacuation routes and allocate resources efficiently to manage the affected population.

5. Conclusion

A comprehensive study conducted in downtown Blida, Algeria, has provided valuable insights into the seismic risk and vulnerability of the area. This study addresses the urgent need for a comprehensive assessment of seismic risk following the devastating earthquake that occurred in 1825. To accomplish this, the study used building typology classification according to Ref. [25] and incorporated the use of SELENA [26], a powerful seismic risk assessment software.

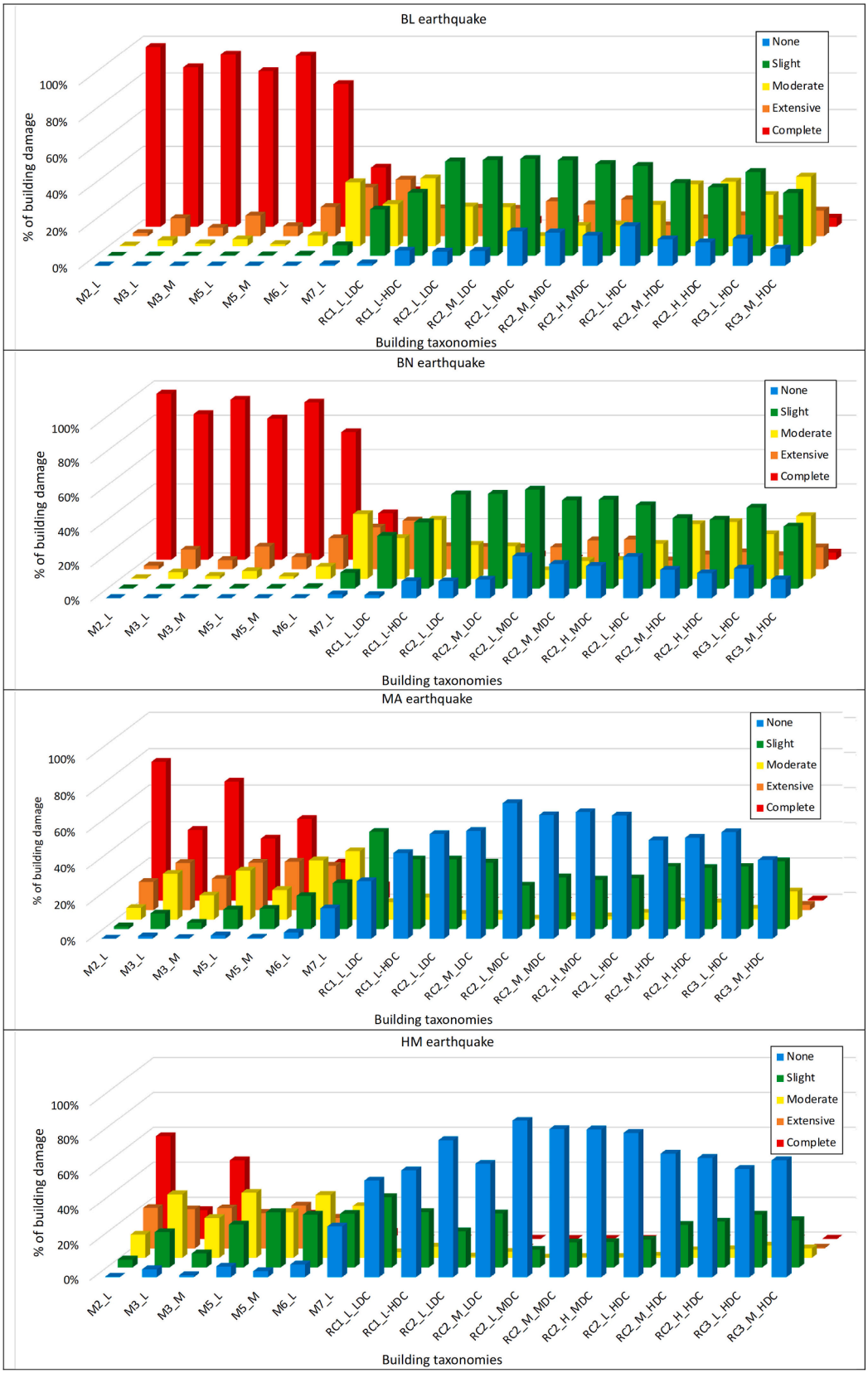
BL earthquake
BN earthquake
MA earthquake
HM earthquake
None
Slight
Moderate
Extensive
Complete
% of building damage
0%
20%
40%
60%
80%
100%
M2_L
M3_L
M3_M
M5_L
M5_M
M6_L
M7_L
RC1_L_LDC
RC1_L-HDC
RC2_L_LDC
RC2_M_LDC
RC2_L_MDC
RC2_M_MDC
RC2_H_MDC
RC2_L_HDC
RC2_M_HDC
RC2_H_HDC
RC3_L_HDC
RC3_M_HDC
Building taxonomies

Fig. 13. Predicted damage probability for the 'none', 'slight', 'moderate', 'extensive' and 'complete' damage classes for the identified model building types in the studied region. The results from the logic tree have been averaged for the three performance point computation methods. BL-Blida Mw7.1; BN-Bouinan Mw7.1; MA-Mouzaia El Affroun Mw6.6 and HM-Hammam Melouane Mw6.5.

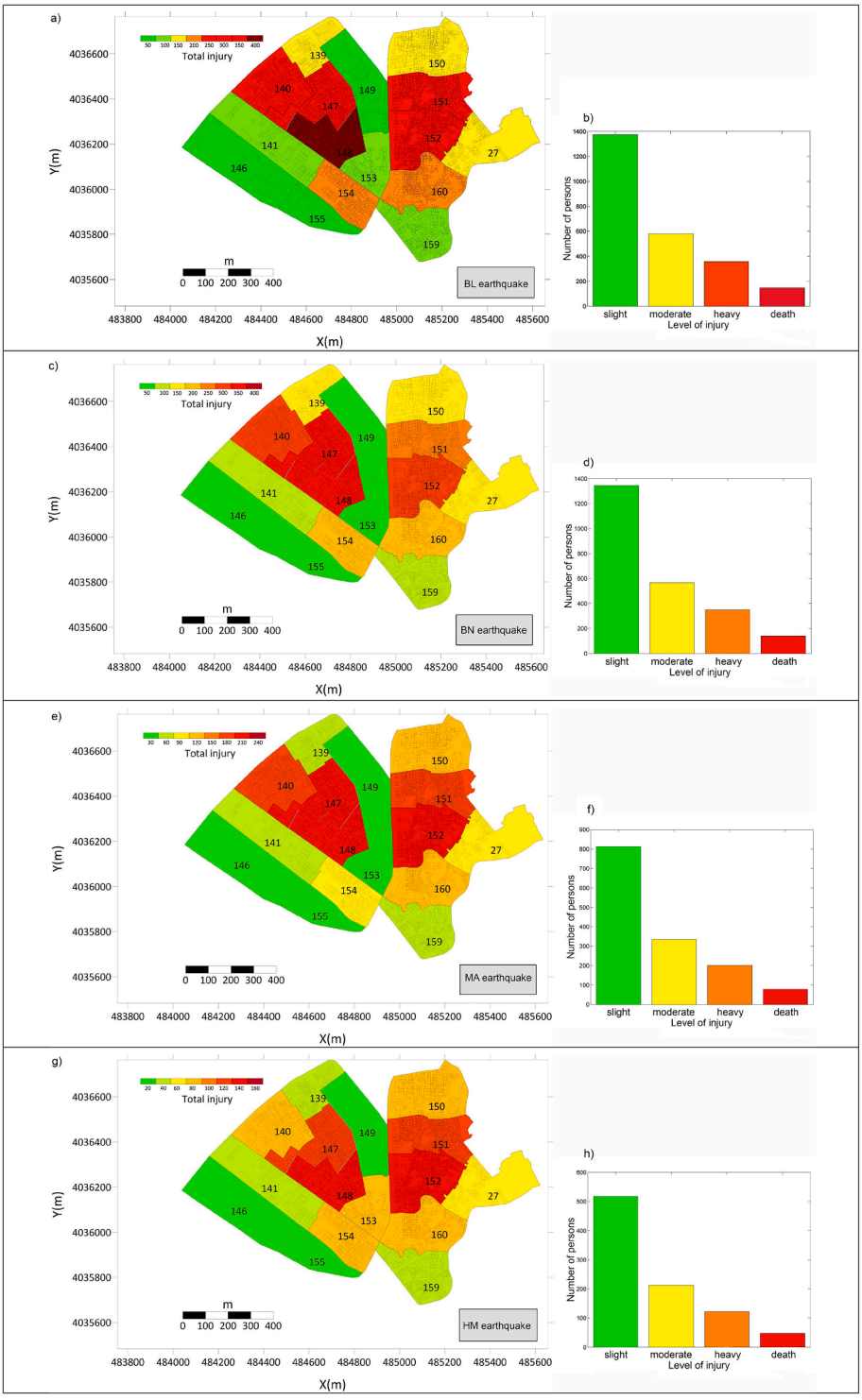

Fig. 14. Distribution of the injured population from the predicted nighttime scenario by considering different severity levels of injuries. For earthquake scenarios a), b) Blida Mw7.1; c), d) Bouainan Mw7.1 , e), f) Mouzaia El Affroun Mw6.6 and g), h) Hammam Melouane Mw6.5.

SELENA played a crucial role in estimating seismic risk by enabling a thorough analysis of earthquake scenarios and their impact on different cadastral sections or geounits. The study divided the area into 16 cadastral and conducted a detailed building inventory that included demographic data, facilitating a comprehensive assessment.

The findings of the seismic risk assessment highlighted the severity and casualties associated with earthquakes in the Blida region. Cadastral sections 148 and 147 emerged as the most affected in all the simulated earthquakes due to the low number of engineering design buildings. Therefore, local authorities should be prepared for targeted risk reduction measures in these areas.

To evaluate the earthquake damage assessment procedures, a sensitivity analysis was conducted, comparing the improved displacement coefficient method (IDCM), the modified capacity spectrum (MADRS), and the nonlinear analysis method (N2). The analysis revealed that the IDCM method exhibits a lower sensitivity to the choice of the ground motion prediction equation. On the other hand, the IDCM method provides the highest results for mean damage ratio, while the N2 method computes the lowest. Regarding the choice of GMPE, if the rupture reaches the city, AK13 provides the lowest mean damage ratio, while LA18 is used if the earthquake is furthest. BR14 consistently provides the highest mean damage ratio, regardless of the earthquake's location. This highlights the importance of using logic trees to define different input parameters with different weights in order to account for the epistemic uncertainties.

Additionally, the study estimated potential human losses in the Blida region, shedding light on the varying levels of impact for different geounits under different earthquake scenarios. This information is crucial for first responders to effectively cope with emergencies.

This comprehensive study significantly enhances our understanding of seismic risk within the urban area of Blida city. The findings not only demonstrate the importance of proactive measures to mitigate the impact of earthquakes but also inform strategies for resilience and loss reduction. The study emphasizes the necessity of implementing targeted risk reduction measures in highly vulnerable cadastral sections.

CRediT authorship contribution statement

Fouzi Bellalem: Writing – review & editing, Writing – original draft, Methodology, Funding acquisition, Formal analysis, Data curation, Conceptualization. **Sergio Molina:** Writing – review & editing, Writing – original draft, Methodology, Investigation, Formal analysis, Conceptualization. **James Daniell:** Writing – review & editing, Writing – original draft, Methodology, Investigation, Conceptualization. **Said Maouche:** Writing – review & editing, Writing – original draft, Investigation, Data curation. **Abdelhak Talbi:** Writing – review & editing, Writing – original draft, Investigation, Data curation. **Mourad Mobarki:** Writing – review & editing, Writing – original draft, Investigation, Data curation. **Hayet Ymmel:** Writing – review & editing, Writing – original draft, Investigation, Data curation. **Hamou Djellit:** Writing – review & editing, Writing – original draft, Investigation, Data curation.

Declaration of competing interest

The authors declare that they have no known competing financial interests or personal relationships that could have appeared to influence the work reported in this paper.

Data availability

Data will be made available on request.

Acknowledgments

We would like to acknowledge the support of the Directorate General for Scientific Research and Technological Development [N°01/CRAAG/DGRSDT] for their financial assistance in conducting this study. The authors express sincere gratitude to the local authorities of Blida for their invaluable support in data acquisition and facilitating access to administrations and building inventory sites. Additionally, the authors would like to extend their thanks to “BET Mahindad Rafik" and “BET MBR ING-Conseils” for their outstanding contributions in creating the building database and conducting the geotechnical study, respectively. We also thank the contributions from two anonymous reviewers which improve the quality of this paper. This publication is dedicated to the memory of Mr. Hamou Djellit, whose early contributions played an instrumental role in the success of this project.

References

[1] A. Perrey, Note sur les tremblements de terre en Algérie et dans l’Afrique septentrionale, 1845–1846. Mém Acad Sci Arts Belles Lettres Dijon, Années. (1847) 299–323 ([in French).
[2] M. Chesneau, Note sur les tremblements de terre en Algérie, Mém Ann Min 9 (1892) 5–46 ([in French]).
[3] R.J. Galbis R, Catalogo sismico de la zone comprendida entrelos meridianos 5° E. y 20° W. de Greenwich y los paralelos45° y 25° N, Imprenta de Ramona Velasco, Madrid, Spain, 1932 ([in Spanish]).
[4] A. Sieberg A, Erdbeben Geographie, Handbuch der Geophysik, Berlin, 1932, pp. 687–1005 ([in German]).
[5] J.P. Rothé, Les séismes de Kherrata et la séismicité del’Algérie, Bull Serv Carte Géol Alger Fourth Ser Géophys 3 (1950) 1–40 ([in French]).
[6] J. Roussel, Les zones actives et la fréquence des séismes en Algérie 1716–1970, Bull. Soc. Hist. Nat. Afr. Nord 64 (1973) 11–227 ([in French]).
[7] H. Benhallou, Les Catastrophes Séismiques de la Région d’Echéliff dans le contexte de la Séismicité Historique de l’Algérie, Thèse de Doctorat es-Sciences, Institut des Sciences de la Terre, Université des Sciences et de la Technologie Houari Boumediène (IST-USTHB), Algiers, Algeria, 1985, p. 294 ([in French]).
[8] N.N. Ambraseys, J. Vogt, Material for the investigation of the seismicity of the region of Algiers, Eur. Earthq. Eng. 3 (1988) 16–29.
[9] A. Harbi A, A. Sebaï, Y. Rouchiche, S. Maouche, F. Ousadou, K. Abbès, D. Ait Benamar, M. Benmedjber, Reappraisal of the seismicity of the southern edge of the Mitidja Basin (Blida region, north-central Algeria), Seismological Research Letter 88 (2017) 1163–1177, https://doi.org/10.1785/0220160217.

[10] F. Bellalem, A. Talbi, H. Djellit, H. Ymmel, M. Mobarki, Seismic hazard assessment in the megacity of Blida (Algeria) and its surrounding regions using parametric-historic procedure, J. Seismol. 22 (2018) 897–908, https://doi.org/10.1007/s10950-018-9740-2.
[11] F. Bellalem, A. Talbi, S. Maouche, A unified Mw parametric earthquake catalog for Algeria and adjacent regions (PECAAR), Mediterranean Geoscience Reviews 4 (2022) 427–443. https://doi:10.1007/s42990-022-00085-w.
[12] K. Tadjer, M. Bensaibi, Earthquake risk assessment of Blida (Algeria) using GIS, Energy Proc. 139 (2017) 645–650, https://doi.org/10.1016/j.egypro.2017.11.266.
[13] M. Hamidatou, B. Sbartai, Deterministic assessment of seismic risk in Constantine city, Northeast Algeria, Nat. Hazards 86 (2017) 441–464, https://doi.org/10.1007/s11069-016-2693-2.
[14] M.B. Sørensen, D.H. Lang, Incorporating simulated ground motion in seismic risk assessment: Application to the lower Indian himalayas, Earthq. Spectra 31 (2012) 71–95, https://doi.org/10.1193/010412EQS001M.
[15] A. Athmani, T.M. Ferreira, R. Vicente, Seismic risk assessment of the historical urban areas of Annaba city, Algeria, Int. J. Architect. Herit. 12 (2018) 47–62, https://doi.org/10.1080/15583058.2017.1370508.
[16] M. Boukri, M.N. Farsi, A. Mebarki, M. Belazougui, M. Ait-Belkace, N. Yousfi, N. Guessoum, D. Ait Benamar, M. Naili, N. Mezouar, O. Amellal, Seismic vulnerability assessment at urban scale: case of Algerian buildings, Int. J. Disaster Risk Reduc. 31 (2018) 555–575, https://doi.org/10.1016/j.ijdrr.2018.06.014.
[17] B. Chaibedra, A. Benanane, Z. Boutaraa, Seismic vulnerability assessment to earthquake at urban scale: a case of Mostaganem city in Algeria, Journal of Disaster Risk Studies 10 (2018), https://doi.org/10.4102/jamba.v10i1.473.
[18] A. Abarca, R. Monteiro, Towards large scale seismic risk assessment in Algeria: case study to the city of Blida, IOP Conf. Ser. Mater. Sci. Eng. 603 (2019) 052065, https://doi.org/10.1088/1757-899X/603/5/052065.
[19] S. Kechidi, J.M. Castro, R. Monteiro, M. Marque, K. Yelles, N. Bourahla, M. Hamdache, Development of exposure datasets for earthquake damage and risk modelling: the case study of northern Algeria, Bull. Earthq. Eng. 19 (2021) 5253–5283 https://doi.org/10.1007/s10518-021-01161-6, 2021.
[20] F. Pavel, R. Vacareanu, Scenario-based earthquake risk assessment for Bucharest, Romania, Int. J. Disaster Risk Reduc. 20 (2016) 138–144, https://doi.org/10.1016/j.ijdrr.2016.11.006.
[21] A. Babič, M. Dolšek, J. Žižmond, Simulating historical earthquakes in existing cities for fostering design of resilient and sustainable communities: the ljubljana case, Sustainability 13 (2021) 7624, https://doi.org/10.3390/su13147624.
[22] E.M. Sherrill, M.W. Hamburger, M.A. Nowicki Jessee, Use of scenario earthquakes for seismic hazard assessment in low-seismicity, stable continental regions: a case study from Indiana, USA, Earthq. Spectra 38 (4) (2022) 2754–2787, https://doi.org/10.1177/87552930221096700.
[23] C. Mesta, D. Kerschbaum, G. Cremen, C. Galasso, Quantifying the potential benefits of risk-mitigation strategies on present and future seismic losses in Kathmandu Valley, Nepal, Earthq. Spectra 39 (1) (2023) 377–401, https://doi.org/10.1177/87552930221134950.
[24] J. Dabbeek, V. Silva, C. Galasso, A. Smith, Probabilistic earthquake and flood loss assessment in the Middle East, Int. J. Disaster Risk Reduc. 49 (2020), 101662 https://doi.org/10.1016/j.ijdrr.2020.101662, ISSN 2212-4209.
[25] S. Lagomarsino, S. Giovinazzi, Macroseismic and mechanical models for the vulnerability and damage assessment of current buildings, Bull. Earthq. Eng. 4 (2006) 415–443, https://doi.org/10.1007/s10518-006-9024-z.
[26] S. Molina, D.H. Lang, C.D. Lindholm, Selena – an open-source tool for seismic risk and loss assessment using a logic tree computation procedure, Comput. Geosci. 36 (2010) 257–269, https://doi.org/10.1016/j.cageo.2009.07.006.
[27] S. Maouche, A. Harbi, The active faults of the Mitidja basin (North Central Algeria): what does the seismic history of the region tell us? A review Euro-Mediterranean Journal for Environmental Integration 3 (2018) 21, https://doi.org/10.1007/s41207-018-0061-1.
[28] M.A. Guemache, H. Djellit, H. Ymmel, S. Gharbi, C. Dorbath, La faille post-astienne de Bouinan - soumaa (région de Blida, bordure sud du bassin de la Mitidja, Algérie) : expression néotectonique et implication dans l'évaluation de l'aléa sismique, Bull. Serv. Geol. Algerie 21 (2010) 75–94.
[29] S. Maouche, M. Meghraoui, C. Morhange, S. Belabbes, Y. Bouhadad, H. Haddoum, Active coastal thrusting and folding, and uplift rate of the Sahel anticline and Zemmouri earthquake area (Tell Atlas, Algeria), Tectonophysics 509 (2011) 69–80, https://doi.org/10.1016/j.tecto.2011.06.003.
[30] A. Harbi, S. Maouche, A. Ayadi, D. Benouar, G.F. Panza, H. Benhallou, Seismicity and tectonic structures in the site of algiers and its surroundings: a step towards microzonation, Pure Appl. Geophys. 161 (2004) 949–967, https://doi.org/10.1007/s00024-003-2502-1.
[31] M.F. Khellif, A. Yelles-Chaouche, Z. Benaissa, F. Semmane, H. Beldjoudi, A. Haned, A. Issaadi, A. Chami, R. Chimouni, A. Harbi, S. Maouche, G. Dabbouz, C. Aidi, A. Kherroubi, The 2016 Mihoub (north-central Algeria) earthquake sequence: seismological and tectonic aspects, Tectonophysics 736 (2018) 62–74, https://doi.org/10.1016/j.tecto.2018.03.015.
[32] A. Ayadi, S. Maouche, H. Harbi, M. Meghraoui, Strong Algerian earthquake strikes near capital city, Eos Transactions American Geophysical Union 84 (2003) 561–568, https://doi.org/10.1029/2003EO500002.
[33] J. Mezcua, J.M. Martinez Solares, Sismidad del Area Ibero Mogrebi, Seccion de Sismologia, Instituto Geografico Nacional, Madrid, Spain, 1983 ([in Spanish]).
[34] D. Benouar D, Materials for the investigation of the seismicity of Algeria and adjacent regions during the twentieth century, Ann. Geophys. 37 (1994), https://doi.org/10.4401/ag-4466.
[35] A.K. Yelles-Chaouche, A. Haned, C. Aidi, H. Beldjoudi, A. Kherroubi, F. Semmane, B.Y.N. Benabdeloued, Y. Larbes, A. Alili, M.F. Khelif, A. Belheouane, The Mw5.0 Hammam Melouane earthquake (north Central Algeria) of 17 july 2013 in the context of the tellian Atlas seismicity, Pure Appl. Geophys. 174 (2017) 1601–1614, https://doi.org/10.1007/s00024-017-1492-3.
[36] D.L. Wells, K.J. Coppersmith, New empirical relationships among magnitude, rupture length, rupture width, rupture area, and surface displacement, Bull. Seismol. Soc. Am. 84 (1994) 974–1002, https://doi.org/10.1785/BSSA0840040974.
[37] R.D. Borcherdt, Estimate of site-dependent response spectra for design (methodology and justification), Earthq. Spectra 10 (1994) 617–654, https://doi.org/10.1193/1.1585791.
[38] R. Dobry, R.D. Borcherdt, C.B. Crouse, I.M. Idriss, W.B. Joyner, G.R. Martin, M.S. Power, E.E. Rinne, R.B. Seed, New site coefficients and site classification system used in recent building seismic code provisions, Earthq. Spectra 16 (2000) 41–67, https://doi.org/10.1193/1.1586082.
[39] D.M. Boore, Estimating VS30 (or NEHRP site classes) from shallow velocity models (depths < 30 m), Bull. Seismol. Soc. Am. 94 (2004) 591–597, https://doi.org/10.1785/0120030105.
[40] T.L. Holzer, A.C. Padovani, M.J. Bennett, T.E. Noce, J.C. Tinsley, Mapping NEHRP VS30 site classes, Earthq. Spectra 21 (2005) 353–370, https://doi.org/10.1193/1.1895726.
[41] A.I. Kanli, P. Tildy, Z. Prónay, A. Pınar, L. Hermann, VS30 mapping and soil classification for seismic site effect evaluation in Dinar region, SW Turkey, Geophys. J. Int. 165 (2006) 223–235, https://doi.org/10.1111/j.1365-246X.2006.02882.x.
[42] M. Ripepe, D. Giustiniani, N. Giovanni, M. Ripepe, A. Lenzi, S. Landi, Shallow depth seismic refraction for engineering site investigation - a solution by micro ordinateurs, in: 6th International IAEG Congress, Sjorgren, Shallow refraction seismic, Chapman and Hall, London, 1984.
[43] D.M. McCann, A. Forster, Reconnaissance geophysical methods in landslides investigation, Eng. Geol. 29 (1990) 59–78, https://doi.org/10.1016/0013-7952(90)90082-C.
[44] S. Kasuga, T. Katsura, Seismic reflection and refraction methods, in: Continental Shelf Limits, Oxford University Press, 2000, https://doi.org/10.1093/oso/9780195117820.003.0017.
[45] F.P. Haeni, Application of Seismic-Refraction Techniques to Hydrologic Studies: U.S, Geological Survey Techniques of Water Resources Investigations, 1988, p. 86 book 2. Chap. D2.
[46] C. Lawton, Component refraction seismic experiment, Can. J. Explor. Geophys. 26 (1990) 7–16.
[47] G. Grelle, F.M. Guadagno, Seismic refraction methodology for groundwater level determination: "Water seismic index.", J. Appl. Geophys. 68 (2009) 301–320, https://doi.org/10.1016/j.jappgeo.2009.02.001.
[48] RPA, Ministère de l'Habitat et de l'Urbanisme, Règles Parasismiques Algériennes RPA 99/Version 2003, Edition CGS..
[49] J. Douglas, Ground motion prediction equations (1964-2021), http://www.gmpe.org.uk, 2021.
[50] N. Laouami, A. Slimani, S. Larbes, Ground motion prediction equations for Algeria and surrounding region using site classification-based H/V spectral ratio, Bull. Earthq. Eng. 16 (2018) 2653–2684, https://doi.org/10.1007/s10518-018-0310-3.

[51] S. Akkar, M.A. Sandıkkaya, J.J. Bommer, Empirical ground-motion models for point- and extended-source crustal earthquake scenarios in Europe and the Middle East, Bull. Earthq. Eng. 12 (2013) 389–390, https://doi.org/10.1007/s10518-013-9461-4.
[52] D.M. Boore, J.P. Stewart, E. Seyhan, G.M. Atkinson, NGA-West2 equations for predicting PGA, PGV, and 5% damped PSA for shallow crustal earthquakes, Earthq. Spectra 30 (2014) 1057–1085, https://doi.org/10.1193/070113EQS184M.
[53] R.J. Budnitz, G. Apostolakis, D.M. Boore, L.S. Cluff, K.J. Coppersmith, C.A. Cornell, P.A. Morris Pa, Recommendations for Probabilistic Seismic Hazard Analysis: Guidance on Uncertainty and Use of Experts, NUREG/CR-6372, Two Volumes, U.S. Nuclear Regulatory Commission, Washington, D.C, 1997.
[54] A.W. Coburn, R.J. Spence, Earthquake Protection, second ed., Hoboken: John Wiley and Sons, Chichester, England, 2002.
[55] ATC, Earthquake Damage Evaluation Data for California, ATC-13, Applied Technology Council, Redwood City, CA, USA, 1985, p. 492.
[56] FEMA, Rapid visual screening of buildings for potential seismic hazards: a handbook, FEMA 154, in: C. RojahnPrincipal Investigator, C. Scawthorn, Co-principal Investigator, Prepared by the Applied Technology Council, Redwood City, CA, second ed., for the Federal Emergency Management Agency, Washington, D.C., USA, 2002 (ATC-21).
[57] K.S. Jaiswal, D.J. Wald, Creating a Global Building Inventory for Earthquake Loss Assessment and Risk Management, U.S, Geological Survey Open-File Report, 2008, p. 103.
[58] S. Brzev, C. Scawthorn, A.W. Charleson, L. Allen, M. Greene, K. Jaiswal, V. Silva, GEM Building Taxonomy Version 2.0, GEM Technical Report 2013-02 V1.0.0, pp. 188, GEM Foundation, Pavia, Italy. https://doi.org/10.13117/GEM.EXP-MOD.TR2013.02..
[59] S.L. Cutter, Vulnerability to environmental hazards, Prog. Hum. Geogr. 20 (1996) 529–539.
[60] S. Freire, C. Aubrecht, Integrating population dynamics into mapping human exposure to seismic hazard, Nat. Hazards Earth Syst. Sci. 12 (2012) 3533–3543, https://doi.org/10.5194/nhess-12-3533-2012.
[61] S. Lagomarsini, S. Cattari S, Seismic vulnerability of existing buildings: observational and mechanical approaches for application in urban areas, in: Chapter Book: "Seismic Vulnerability of Structures", John Wiley & Sons, Inc, 2013.
[62] FEMA, Improvement of Nonlinear Static Seismic Analysis Procedures, Applied Technology Council, California, USA, 2005 Technical report FEMA-440.
[63] P. Fajfar, A nonlinear analysis method for performance-based seismic design, Earthq. Spectra 16 (2000) 573–592, https://doi.org/10.1193/1.1586128.
[64] C.A. Kircher, A.A. Nassar, O. Kustu, W.T. Holmes, Development of building damage functions for earthquake loss estimation, Earthq. Spectra 13 (1997) 663–683, https://doi.org/10.1193/1.1585974.
[65] D.H. Lang, S. Molina, C.D. Lindholm, Towards near-real-time damage estimation using a CSM-based tool for seismic risk assessment, J. Earthq. Eng. 12 (2008) 199–210, https://doi.org/10.1080/13632460802014055.
[66] D.L. Lang, S. Molina-Palacios, C.D. Lindholm, S. Balan, Deterministic earthquake damage and loss assessment for the city of bucharest, Romania, J. Seismol. 16 (2012) 67–88, https://doi.org/10.1007/s10950-011-9250-y.
[67] E. Erduran, D.H. Lang, Sensitivity of Earthquake Risk Models to Uncertainties in Hazard, Exposure and Vulnerability Parameters, vol. 9, NED University Journal of Research, Karachi (Pakistan), 2012, pp. 73–86.
[68] FEMA, HAZUS-MH.Multi-hazard Loss Estimation Methodology, Technical manual, Washington DC, USA, 2003.